Macromolecular Materials and Engineering
www.mme-journal.de

A Theoretical and Experimental Analysis of the Effect of Nanoclay on Gas Perm-Selectivity of Biodegradable PLA/EVA Blends in the Presence and Absence of Compatibilizer

Navid Karimpour-Motlagh, Abolfazl Salehi Moghadam, Hossein Ali Khonakdar, Seyed Hassan Jafari, Udo Wagenknecht, Sina Farahani Kasbi, Shahrokh Shojaei, and Ramin Mirzaee*

Poly (lactic acid) (PLA)-based compounds are widely used in thin-film and food packaging industries. Herein, PLA/ethylene vinyl acetate copolymer (EVA)/nanoclay nanocomposites are prepared in various compositions by melt blending. The gas permeability against N_2, CO_2, and O_2 gases is determined as a function of composition and morphology of the nanocomposites. Inclusion of high aspect ratio of platelet-like nanoclay to the blend reduces the gas diffusion. The best barrier properties against all gases is observed on introducing 5 wt% poly(ethylene/n-butyl acrylate glycidyl methacrylate) copolymer as compatibilizer to the PLA/EVA/nanoclay (75/25/5) system. The scanning and transmission electron microscopic analyses and wide-angle X-ray scattering studies reveal that inclusion of compatibilizer to the filled-blends improves the blend morphology, dispersion state, and intercalation level of clay platelets which are preferably localized at the interface of the blend. Analysis of selectivity parameter (α) shows the lowest O_2 permeability and the highest $\alpha_{CO2/N2}$ and $\alpha_{O2/N2}$ values for the compatibilized filled-blend (75/25/5/5). In situ aspect ratio of clay and the degree of intercalation are theoretically evaluated based on the permeability data using various empirical models. It is found that the compatibilized filled-blend has the highest aspect ratio and intercalation level that are responsible for the optimum perm-selectivity performance.

1. Introduction

Considering fossil fuel consumption and environmental contaminants, packaging industry tends to use biodegradable and eco-friendly polymers instead of petroleum-based conventional plastics such as polyethylene (PE), polypropylene (PP), polyvinyl-chloride (PVC), and polyamide (PA) that are widely employed in the packaging industry.[1–4] Bio-based, semicrystalline poly(lactic-acid) (PLA) is one of the widespread materials which is used as the biodegradable polymer in the packaging application, tissue engineering, drug delivery systems, etc.[5–9] PLA, due to its low cost of polymerization, appropriate thermal behavior, excellent barrier properties, high strength, and stiffness, is richly applicable but have noticeable drawbacks such as brittleness and hydrolysis.[10] Blending of PLA with a tough or rubbery polymer combined with nanoparticles inclusion are quietly accessible approach to cover its shortages. There are several reports about blending

N. Karimpour-Motlagh, Prof. H. A. Khonakdar
Department of Processing
Iran Polymer and Petrochemical Institute
P. O. Box 14965/115, Tehran 1497713115, Iran
E-mail: hakhonakdar@gmail.com

A. S. Moghadam, Prof. S. H. Jafari, S. F. Kasbi
School of Chemical Engineering
College of Engineering
University of Tehran
P. O. Box 11155-4563, Tehran 1417466191, Iran

The ORCID identification number(s) for the author(s) of this article can be found under https://doi.org/10.1002/mame.202000433.

After first online publication Projekt Deal funding statement has been added on 28 October 2020.

DOI: 10.1002/mame.202000433

Prof. H. A. Khonakdar, Prof. U. Wagenknecht
Leibniz Institute of Polymer Research Dresden
D-01067, Dresden, Germany

S. Shojaei
Department of Biomedical Engineering
Islamic Azad University
Central Tehran Branch, P. O. Box 13185/768, Tehran 13117773591, Iran

S. Shojaei
Stem cells Research Center, Tissue Engineering and Regenerative Medicine Institute
Islamic Azad University
Central Tehran Branch, P. O. Box 13185-768, Tehran 13117773591, Iran

R. Mirzaee
Department of Polymer Engineering and Color Technology
No. 350, Hafez Ave., Valiasr Square, Tehran 15875-4413, Iran

of PLA with various biodegradable or non-biodegradable (co) polymers.[2,6,11,12] Among them ethylene-*co*-vinyl acetate (EVA) is a suitable material for blending with PLA, since it compensates the brittleness of PLA due to its high toughness and flexibility.[6,13,14] It is thought that the blend of PLA/EVA is generally immiscible, but the compatibility of the blend depends on the vinyl acetate (VA) content which increases with respect to the VA content.[15] There are a few reports on using different agents as a compatibilizer specially between the PLA and EVA.[3,5,16,17] Less Obviously, using compatibilizer will cause a higher level of intercalation of clay in a polymeric matrix which leads to a higher in situ aspect ratio and a significant enhancement of barrier property.[18] This phenomenon is due to creation of a strong polymer–filler interface and a proper filler dispersion in the polymer matrix[19] which directly affect the gas transport properties.

An acceptable gas barrier performance which needs to be boosted is recognized as a crucial factor in packaging films industry. For having an appropriate film for food packaging, O_2 permeability through the film must be considerably low and also the film must allow CO_2 to diffuse out of the package. Furthermore, the permeability of N_2 as an inert gas helps to reduce the degeneration rate of the food.[2] One of the commonly used manners to promote gas barrier performance of a polymer is to add platelet nanofillers like nanoclay.[20–23] Clay has a high aspect ratio owing 2D platelet-like structure, which can prolong the gas diffusion pathway by a mechanism known as tortuosity.[24] In this context, gas diffusion will be delayed and overall permeation can be reduced. By incorporating nanoclay platelets, besides the gas permeability reduction, one can also expect promising mechanical properties for nanocomposite.[3,25] Mainly, diffusivity and solubility are two parameters in permeation characteristics that are kinetic and thermodynamic parameters; relating to the gas mobility through the filler and the gas solubility in filler/polymer of the filler–polymer interface.[18,20] The interfacial adhesion between filler and polymer is another factor which can affect the gas permeation.[26] Recently, the role of interfacial behavior of graphene oxide on gas permeation through rubber composites has been scrupulously identified by some researchers.[27] The results showed that increase in rubber–filler interactions leads to strong adhesion at the interface, thicker interphase layers, and more bound rubber. This parameter, which can be altered either by functionalization or compatibilization, has been considered as an important factor similar to tortuosity effect. Creation of a strong interface depends on the compatibility of the filler–polymer, nature of side chain, or backbone groups of the matrix and also crystallinity.[28,29] Crystallinity, especially in plastic materials can cause improvement in gas barrier property due to chain packing.[9,30] In a crystalline polymer, gas molecules cannot easily diffuse or dissolve into the crystalline domain, so the solubility and diffusion coefficient are small.[2] Also, it has been reported that with rise of VA content in EVA, polarity increases which positively affects clay dispersion and improves its degree of exfoliation/or intercalation. Moreover, the degree of intercalation or exfoliation of clay directly affects the in situ aspect ratio of clay which itself can be affected by mixing method[15] .

For estimating the in situ aspect ratio of embedded platelet filler in a matrix, there are vast types of phenomenological models which are available in open literature.[31,32] The Nielsen,[33] Cussler et al., and Bharadwaj models[34,35] are the most widely employed ones in the case of platelet-like fillers.[36] Usually, the value of in situ aspect ratio is lower than that of the intrinsic particle aspect ratio because of the stacking and formation of tactoids resulting from the agglomeration and/or incomplete exfoliation of filler in the matrix.[18]

In our previous works, we deeply investigated the localization of nanoclay in PLA/EVA/nanoclay nanocomposites and also performed an in-depth analysis of micromechanisms of the mechanical property alternations of the nanocomposites.[3,5]

In continuation, here we perform a theoretical and experimental analysis of effect of nanoclay on gas perm-selectivity of biodegradable PLA/EVA blends in the presence and absence of compatibilizer. An attempt is made to establish a correlation between the perm-selectivity and microstructural characteristics of the developed systems.

2. Experimental Section

2.1. Materials

PLA (Ingeo 4043D; density = 1.21 g cm^{-3}, M_w = 100 000 g mol^{-1}, L/D isomeric forms = 98/2) was purchased from Nature Works, USA. EVA (UL00218 grade; density = 0.94 g cm^{-3}, MFI at 190 °C and 2.16 kg = 1.7 g/10 min and VA content of 18 wt%) was obtained from Exxon Mobile Chemical Company. Elvaloy PTW as compatibilizer, which is a terpolymer of ethylene, butyl acrylate, and glycidylmethacrylate, was purchased from Dupont, USA (density = 0.94 g cm^{-3}, MFI at 190 °C, and 2.16 kg = 10 g/10 min). Commercial clay Cloisite 30B (MMT-Na^+ modified with bis-(2-hydroxyethyl) methyl tallow alkyl ammonium cations, wet density = 1.77 g cm^{-3}) was purchased from Southern Clay Products, USA. All components were dried at 80 °C for 4 h in a vacuum oven before the melt mixing stage.

2.2. Sample Preparation

A corotating twin screw extruder Micro 27 (Leistritz, Nuremberg) equipped with gravimetric and a strand pelletizer was used to fabricate the composites. All runs followed by a screw speed of 150 rpm and throughput of 10 kg h^{-1}. The extrusion temperature profile was set from 160 to 190 °C from hopper to die. Afterward, the obtained pellets were vacuum dried at 50 °C for 24 h for characterization and testing. The different compositions of the prepared sample are listed in **Table 1**. For gas permeation measurements, thin films with a thickness of 150–200 μm were fabricated by compression molding using a hot press (20 MT minilab, Labtech, Thailand) under a pressure of 15 MPa for 2 min. For each specimen, an equal weight of 3 g was preheated at 180 °C for 1 min in a thin film cavity, to obtain the thin film. The name, composition, filler content and compatibilizer loading of samples are reposted in Table 1. It should be mentioned that according to the previous studies on the similar blend nanocomposite systems[2,3] only a set of optimized systems with a fixed clay loading of 5 wt% were chosen to investigate the role of blend composition, clay, and compatibilizer on the gas perm-selectivity of the developed blend nanocomposites. Higher loadings of clay lead to server reduction in gas permeability of these materials.

Table 1. PLA/EVA hybrids with different compositions.

Sample	Sample coding	Filler loading [wt%]	Components composition		
			PLA	EVA	PTW
PLA	PLA	0	100	0	0
EVA	EVA	0	0	100	0
PLA/EVA-1	75/25	0	75	25	0
PLA/EVA-2	25/75	0	25	75	0
PLA/EVA/Cloisite 30B-1	75/25/C5	5	75	25	0
PLA/EVA/Cloisite 30B-2	25/75/C5	5	25	75	0
PLA/EVA/Cloisite 30B/PTW	75/25/C5/Co5	5	75	25	5

2.3. Morphology

In order to monitor the state of clay dispersion, the effect of compatibilization and blend morphology as well as crystallinity and its changes, scanning electron microscopy (SEM), transmission electron microscopy (TEM) images, wide-angle X-ray scattering (WAXS), and differential scanning calorimetry (DSC) were implemented.

2.3.1. Scanning Electron Microscopy (SEM)

Scanning electron microscopy (SEM; NEON 40 EsB, Carl Zeiss, Oberkochen, Germany) was used to characterize the morphology and state of dispersion in blends. An extruded strand of each sample after drying was cryo-fractured in liquid nitrogen. The sample was sputter coated with 3 nm of platinum for good conductivity of electron beam.

2.3.2. Transmission Electron Microscopy (TEM)

Transmission electron microscopy (TEM; Philips EM208 microscope, 100 kV, Netherlands) was employed to elucidating the dispersion quality of nanoclay within the matrix and nanostructures of the nanocomposites. The sample was microtomed at –100 °C.

2.3.3. Wide-Angle X-Ray Scattering (WAXS)

Wide-angle X-ray scattering (WAXS) analysis was performed on injection molded specimens with XRD (Seifert-FPM Freiberg/Sa 3003, Germany) using Cu Kα X-ray radiation source over a 2θ range of 0.5 to 10°, with a scanning rate of 1° min^{-1} and a step size of 0.05° at 40 kV and 30 mA.

2.4. Gas Permeation Measurements

The permeability coefficient of CO_2, O_2, and N_2 gases in neat PLA, EVA, and their nanocomposites was measured using a gas permeability apparatus (Coesfeld, GDP-C, Germany), ASTM D1434 82 (M). The permeation measurements were performed at room temperature (25 °C) and pressures (3 bars). It is worth mentioning that the measured value is based on the barrer (1 barrer = 3.348×10^{-16} mol m (m^2 s Pa)$^{-1}$. The schematic diagram of experimental setup for the single gas permeation depicts in **Figure 1**. In order to ensure the reproducibility of the results, the permeability of each gas through each sample was measured three times and the average values with standard deviations in the range of 4–6% were reported. Besides the dry state, the experiment was performed at the different relative humidity of 20%, 40%, 60%, 80%, and 100% for investigating the effect of moisture.

3. Results and Discussion

3.1. Morphology

The final properties like gas permeability and particularly selectivity of a multicomponent system strongly depend on its morphology. Correspondingly, morphology of polymer blend composites, i.e., size, volume fraction, and spatial distribution of the dispersed phase, is a key factor in controlling the gas perm-selectivity of the hybrid materials. Thus, development of

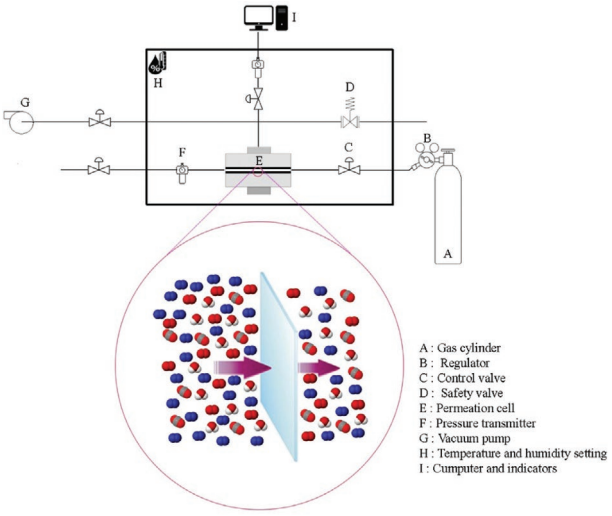

Figure 1. Schematic of gas permeation measurement.

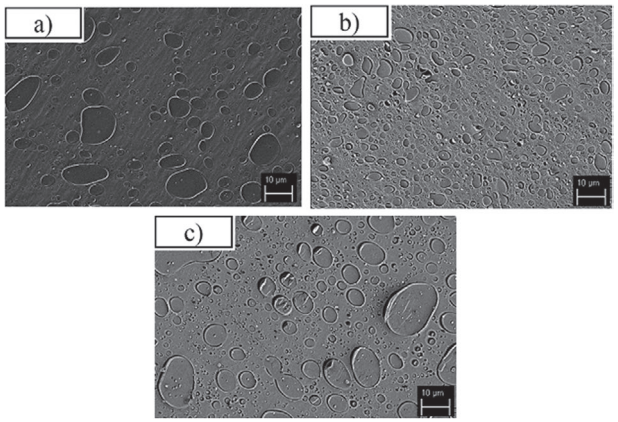

Figure 2. SEM micrographs of PLA/EVA blends in the presence and absence of clay and compatibilizer: a) PLA/EVA (75/25), b) PLA/EVA/Cloisite 30B (75/25/C5), and c) PLA/EVA/Cloisite 30B/PTW (75/25/C5/Co5).

a polymer system with improved permeability requires detailed knowledge of the inter-relationships between the microstructure and the permeability of the system.

A detailed morphological investigations on PLA/EVA blends and their corresponding nanocomposite systems is reported in our previous works.[3,5] Here, we briefly present the relevant morphological information needed to explain the perm-selectivity behavior of the system from microscopic point of view. In this context, the microstructure of PLA/EVA (75/25) blend and its nanocomposites, i.e., PLA/EVA/Cloisite 30B (75/25/C5) and PLA/EVA/Cloisite 30B/PTW (75/25/C5/Co5) are shown in **Figure 2**a–c. The matrix–droplet morphology is observed in the all samples with EVA and PLA as dispersed and matrix phases, respectively. These micrographs clearly display that the EVA dispersed droplets have been distributed uniformly within the PLA matrix. By comparing the droplet size in the SEM micrographs (**Table 2**), the average radius of the EVA domains is about 2.0 μm for the PLA/EVA blend. When 5 wt% of Cloisite 30B is added to this blend it leads to reduction of EVA dispersed droplets to about 1.2 μm possibly due to changing the viscosity ratio of the blend. The change in viscosity ratio may in turn augment the viscose forces needed to break the dispersed phase into smaller droplets. When PTW, as compatibilizer, is added to the blend nanocomposite (75/25/C5/Co5), the EVA dispersed droplets are elongated and tend to form larger elliptical shape with a mean average size of about 1.4 μm implying that the efficiency of the compatibilizer has been reduced in

Table 2. The quantitative values obtained from SEM micrographs of neat blends and corresponding nanocomposites.

Sample name	R_n [μm]	R_v [μm]	PDI = R_v/R_n
75/25	2.0	5.5	2.8
25/75	1.4	2.2	1.6
75/25/C5	1.2	1. 6	1.4
25/75/C5	1.3	2.0	1.6
75/25/C5/Co5	1.4	1.9	1.4

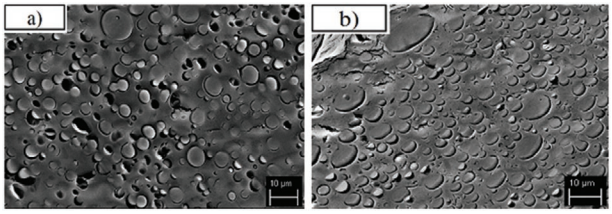

Figure 3. SEM micrographs of a) PLA/EVA(25/75) and b) PLA/EVA/Cloisite 30B (25/75/C5).

the presence of clay. Similar results were reported by other researchers.[37].

The SEM micrographs displaying the morphology of PLA/EVA (25/75) blend and the corresponding nanocomposite, i.e., PLA/EVA/Cloisite 30B (25/75/C5) sample are presented in **Figure 3**a,b. The quantitative data regarding PLA droplet size and size distribution are reported in Table 2. It is evident that the EVA-rich blend (25/75) has smaller droplet size (1.4 μm) than that of the PLA-rich blend (75/25) which was attributed to viscosity difference between the two components.[4] With incorporating 5 wt% clay to PLA/EVA (25/75) blend the PLA droplet size becomes slightly smaller (1.3 μm) than that of the neat blend. This phenomenon has been explained on the basis of clay localization/migration studied by the TEM investigation. A brief summary of the main TEM findings will be presented subsequently.

TEM and XRD investigations on PLA/EVA blend nanocomposites were carried out to reveal the clay dispersion, exfoliation/intercalation states and its partition in the blend phases, as main controlling factors, which affect gas barrier properties of the final system.[38] The TEM micrographs of PLA/EVA (75/25) blend nanocomposites in the presence and absence of compatibilizer are depicted in **Figure 4**a,b. Combination of mainly intercalated and some exfoliated structures are seen in both the systems confirmed by XRD analysis too (Figure 4c). It is also seen that clay particles are mostly localized in the PLA phase with some portion remaining at the blend interface. The localization of clay particles within PLA matrix will be probed from thermodynamic aspects subsequently. Incorporation of the compatibilizer to the nanocomposite system results in migration of clay particles from PLA matrix toward blend interface (Figure 4b). Moreover, the compatibilizer has a significant effect on dispersion state and intercalation level of clay particles. These morphological features of the clay localization and migration can directly affect the gas transport properties of the system which will be discussed in the next sections.

The selective localization of the nanoparticles in a polymer blend is due to the balance of interfacial energies between different components of the system. To confirm the previous results obtained by SEM and TEM on the localization of nanoclay, the interfacial energies can be estimated by the harmonic-mean equation

$$\gamma_{12} = \gamma_1 + \gamma_2 - 4\left(\frac{\gamma_1^d \gamma_2^d}{\gamma_1^d + \gamma_2^d} + \frac{\gamma_1^p \gamma_2^p}{\gamma_1^p + \gamma_2^p}\right) \quad (1)$$

where γ_{12} is the interfacial tension between two phases (subscripts 1 and 2), and γ^d and γ^p are the dispersive and polar components of the surface energy for both the constituents.

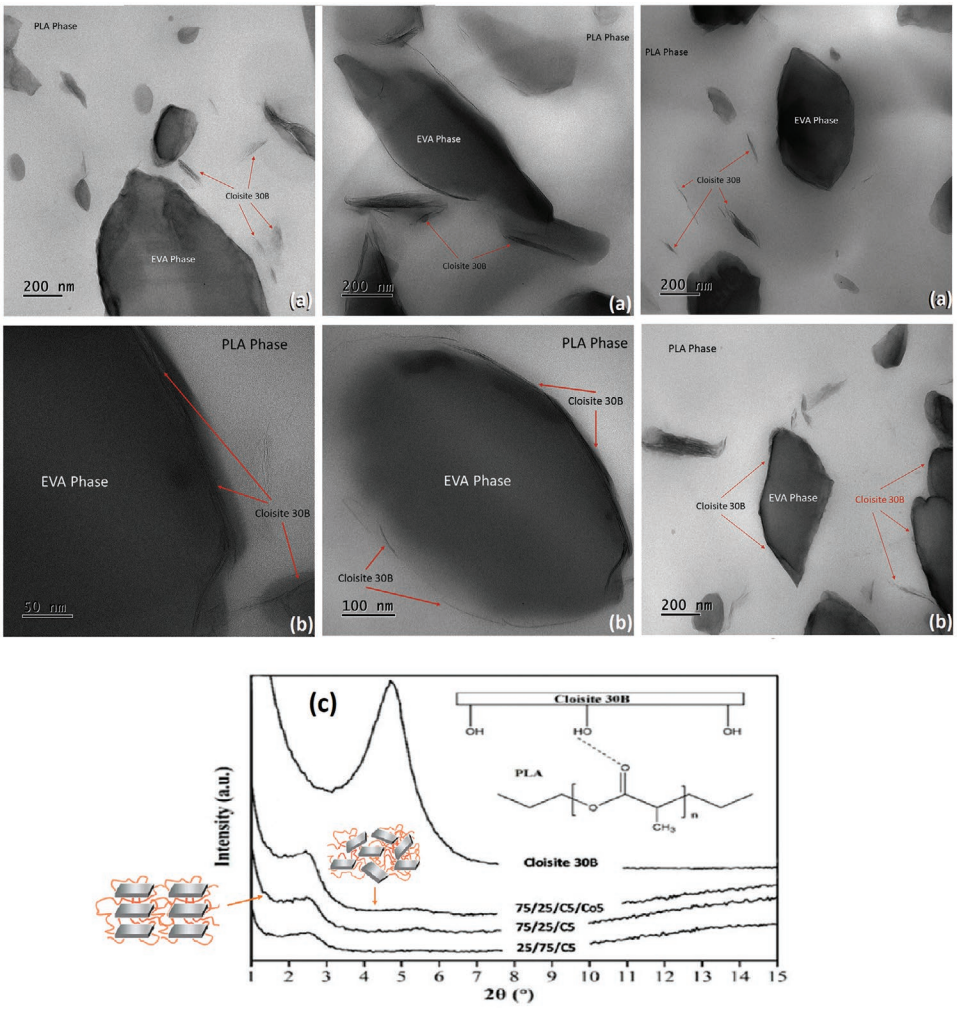

Figure 4. TEM image of a) 75/25/C5, b) 75/25/C5/Co5, and c) WAXS patterns of Cloisite 30B, 75/25/C5, 25/75/C5, and 75/25/C5/Co5.

Classical thermodynamics is often used to predict the location of fillers in blends of immiscible polymers. In the equilibrium state, the location of a filler in a polymer blend can be predicted by minimizing the interfacial tension. From Young's equation, the location of the nanofillers in the equilibrium state can be estimated by calculating the wetting coefficient (ω_a) as follows

$$\omega_a = \frac{\gamma_{PLA-Clay} - \gamma_{EVA-Clay}}{\gamma_{PLA-EVA}} \quad (2)$$

where $\gamma_{Clay-PLA}$, $\gamma_{Clay-EVA}$, and $\gamma_{PLA-EVA}$ are the interfacial energies between clay and PLA, clay and EVA, and PLA and EVA phases, respectively. The values of the wetting coefficient give three possibilities for the location of the clay in the blend system (**Figure 5**).

The wetting parameters (ω_a) from the Young's equation were determined by using the interfacial tension between the components. Hence, based on the surface energy values presented in **Table 3** the interfacial tension values between PLA–EVA ($\gamma_{PLA-EVA}$), PLA–clay ($\gamma_{PLA-Clay}$), and EVA–clay ($\gamma_{EVA-Clay}$) are equal to 1.50, 0.23, and 2.19 (mN m^{-1}), respectively. Eventually, ω_a of the mentioned system is −1.30; therefore, thermodynamically the clay platelets are preferably located at PLA phase that is inline with the TEM findings.

3.2. Gas Transport Properties

3.2.1. Gas Permeability

For obtaining comprehensive information about the gas transport properties of the described materials, single gas tests were carried out on a time-lag measurement machine. Permeability of the neat PLA and EVA components, their neat blends and the clay-containing blend systems against N_2, O_2, and CO_2 gases are presented in **Figure 6** and then the values of permeability and permeability reduction of whole samples compared to PLA and EVA-rich blends are tabulated in **Table 4**. It is seen that among all gases, N_2 exhibits the lowest diffusion in all samples which can be attributed to its inert nature while CO_2 shows the highest diffusion due to its polar nature. The gas

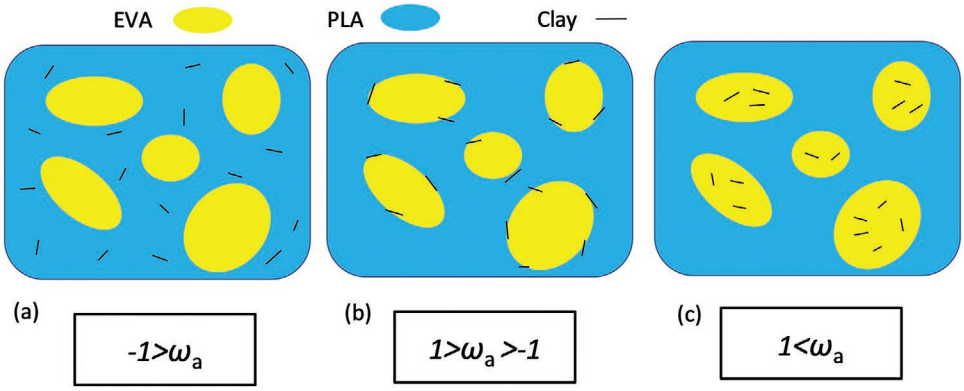

Figure 5. Schematic representation of different possibilities for clay distribution in the PLA/EVA blend.

permeability coefficients of the neat PLA against all gases (N_2, O_2, and CO_2) are considerably lower than that of the neat EVA. This is related to the intrinsic low permeability of PLA due to its molecular structure. Another notable reason is the glass transition temperatures of the neat PLA and EVA which remain at the glassy and rubbery states, respectively at the measurement temperature (25 °C). Consequently, EVA chains have higher chain mobility than that of PLA[2] and this difference in mobility in turn affects the barrier properties of these materials. Hence, PLA has more desirable barrier properties than that of EVA. Incorporation of EVA with intrinsic high permeability to PLA increases the PLA permeability against all the gases to a large extent beyond the simple mixing rule implying that the permeability in this system is mainly controlled by EVA component of the blend. Therefore, the EVA-rich (25/75) blend has significantly higher gas permeability than that of the PLA-rich (75/25) blend. The permeability of the EVA-rich blend is almost near to the permeability of the neat EVA confirming that the permeability in PLA/EVA system is mainly controlled by EVA component of the blend.

It is known that incorporation of clay to a polymer generally reduces the gas permeability against all the gases due to creation of a tortuous path and decrease in free volume fraction that prolongs the gas diffusion pathway. However, this behavior may change when one deals with an immiscible blend system in which blend morphology plays crucial role in controlling permeability.

From Figure 6 it is seen that when clay is loaded to the PLA-rich blend the permeability of the blend against all the gases reduces however, it has no significant effect on the permeability of EVA-rich blend. The observed reduction in the permeability of PLA-rich system can be explained by localization of nanoclay. As discussed earlier, the clay platelets are preferably localized at PLA phase of the blend which can create a tortuous path against infiltration of the gases through the PLA matrix. As confirmed by the SEM results, the localization of nanoclay within PLA matrix can also decrease the size of dispersed EVA domains. This refinement of morphology can also be responsible for the observed reduction of permeability. On the other hand, since clay particles are localized in PLA phase they have no discernible effect on reduction of permeability in the EVA-rich system.

From the data presented in Figure 6, it is also possible to infer the influence of compatibilizer on permeability behavior of PLA/EVA systems. It is seen that inclusion of compatibilizer to PLA-rich nanocomposite (75/25/5) slightly improves its gas barrier properties. This reduction can be explained by the role of compatibilizer in improving dispersion of clay platelets and their migration toward blend interface as confirmed by XRD and microscopic observations. The presence of clay platelets in the interface decreases the gas

Table 3. Surface free energies and dispersive and polar components of the materials.

Material	γ^p [mJ m^{-2}]	γ^d [mJ m^{-2}]	γ[mJ m^{-2}]	Ref.
EVA	6.51	27.9	34.41	[39]
PLA	16.54	2.53	19.07	[40]
Cloisite 30B	12.60	22.40	35	[40]

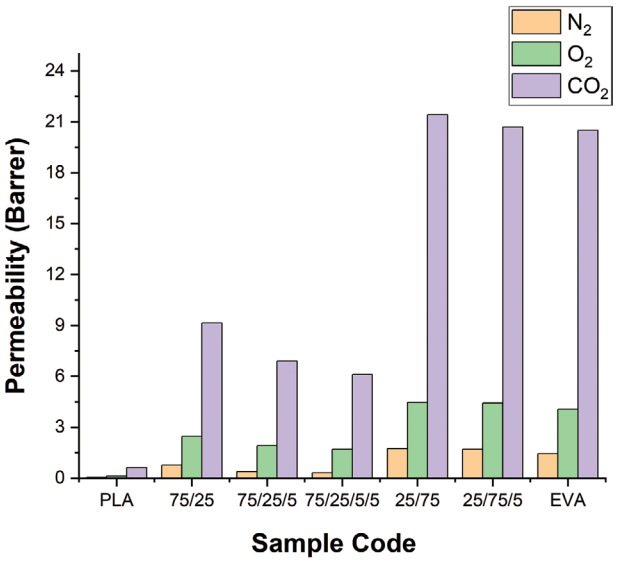

Figure 6. Permeability of neat PLA, EVA components, neat blends, and filled blends.

Table 4. Permeability of samples and permeability reduction for samples in comparison to PLA- and EVA-rich blends.

				Permeability reduction [%]					
				Compared to PLA-rich blend			Compared to EVA-rich blend		
	P_{O2}	P_{N2}	P_{CO2}	O_2	N_2	CO_2	O_2	N_2	CO_2
PLA	0.12	0.05	0.62	–	–	–	–	–	–
75/25	2.45	0.76	9.14	–	–	–	–	–	–
75/25/5	1.9	0.38	6.9	22.45	50	24.51	–	–	–
75/25/5/5	1.7	0.31	6.1	30.61	59.21	33.26	–	–	–
25/75	4.47	1.73	21.42	–	–	–	–	–	–
25/75/5	4.42	1.7	20.7	–	–	–	1.12	1.73	3.36
EVA	4.05	1.44	20.5	–	–	–	–	–	–

transport throughout the interfacial region. Since clay had no discernable effect on permeability of EVA-rich system therefore it is expected that the compatibilizer plays no role in permeability behavior of EVA-rich system.

3.2.2. Gas Selectivity

Figure 7 shows the selectivity of both CO_2/N_2 and O_2/N_2 for the neat PLA and EVA, and their blends and nanocomposites. It is seen that the selectivity of CO_2/N_2 in all samples is greater than the selectivity of O_2/N_2. This is due to the fact that, in comparison with O_2, the CO_2 has higher diffusion in the samples. The selectivity of both CO_2/N_2 and O_2/N_2 for the neat EVA is slightly higher than that for PLA. The nonpolar nature of EVA and CO_2 allows the CO_2 gas to pass though the EVA more than the PLA. The blends (PLA-rich and EVA-rich) exhibit almost the same gas selectivity in between those of the neat components. However, the selectivity in both the blends is lower than the mixing rule indicating that the immiscible nature of these blends plays some roles in reducing the gas selectivity due to the poor blend interface. Incorporation of clay to the blends improves the gas selectivity in the PLA-rich system while it has no discernable effect on gas selectivity in the EVA-rich system. As discussed above, this difference in the gas selectivity can be attributed to the localization of clay platelets in the PLA phase. The improvement of gas selectivity in the presence of clay has been reported to the role of clay in increasing gas surface adsorption and enhancing specific interactions with gases.[41] Incorporation of compatibilizer to the PLA-rich system further improves the gas selectivity due to polar nature of the compatibilizer, interface modification and improvement of clay dispersion within the PLA matrix.

Comparison of the permeability and gas selectivity of all the studied samples indicate that the compatibilized filled PLA-rich has the lowest O_2 permeability and the highest CO_2/N_2 selectivity among all the samples making it the most suitable candidate for food packaging applications. For such applications, low O_2 and high CO_2 permeability is needed to preserve the food against O_2 diffusion and allow CO_2 to pass through out of the package. Additionally, the diffusion of N_2 reduces the degeneration of food.[2]

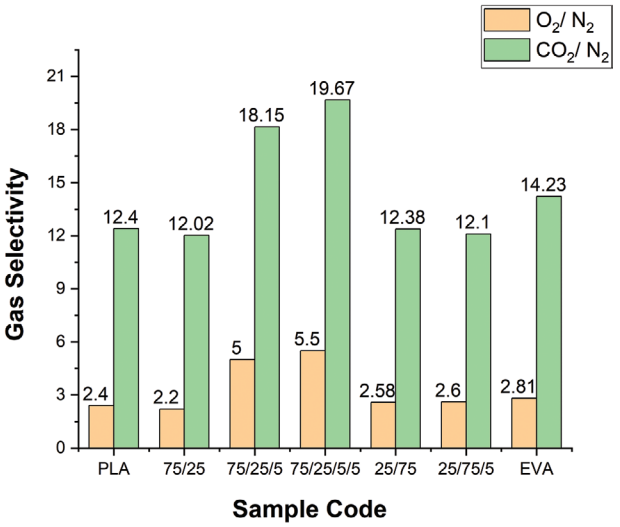

Figure 7. O_2/N_2 and CO_2/N_2 gas selectivity in neat PLA, EVA components, neat blends, and the filled blends.

3.2.3. Influence of Relative Humidity on Gas Permeability

Environmental factors like relative humidity play an important role in packaging industry and they may affect the barrier properties of polymers.[42] So, it is important to investigate gas permeability on different range of moisture as a function of relative humidity. **Figure 8** summarizes gas permeability in humid conditions for PLA/EVA blends and their nanocomposites in the presence and absence of compatibilizer. As shown, the permeability of all the samples against all the gases reduces in the humid conditions and the order of gases diffusion remain the same. Similar to the dry condition, the PLA-rich system has significantly lower permeability than that of the EVA-rich system in the humid conditions and the barrier properties of clay again plays important role in reducing the gas diffusion through the filled systems particularly in the PLA-rich system. Moreover, the results show that the PLA-rich system is slightly more sensitive toward relative humidity as compared to the EVA-rich system attributed to more hydrophilic nature of PLA. In the PLA-rich

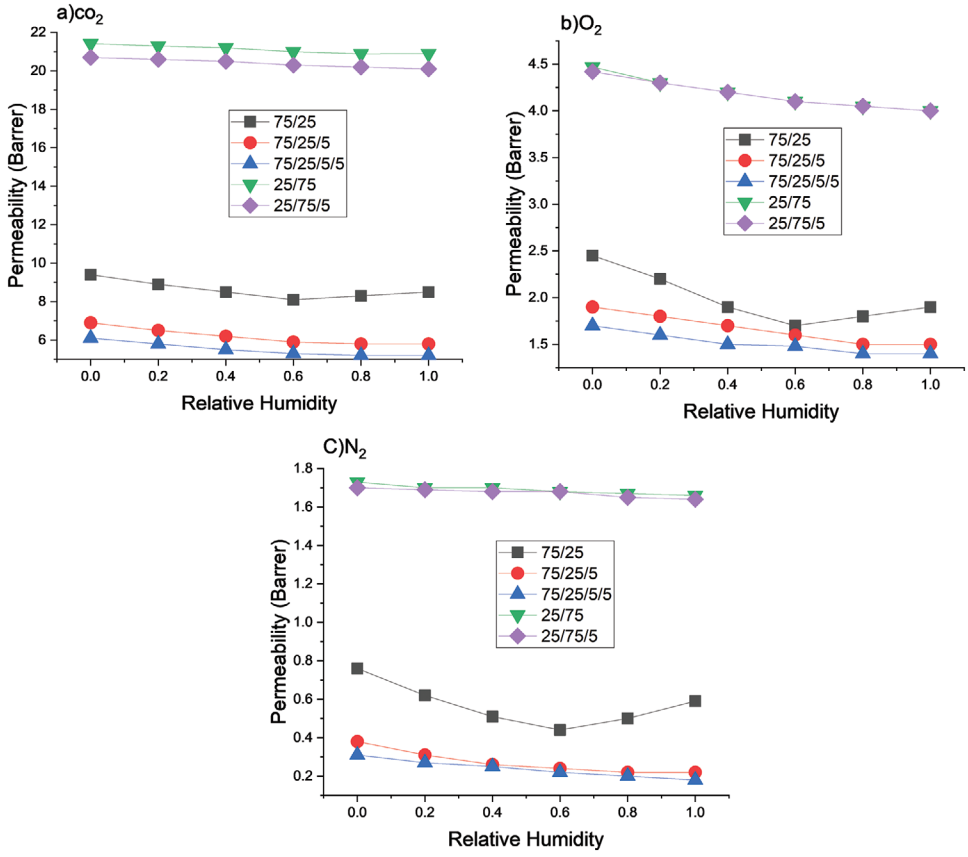

Figure 8. Gas permeability of samples at different relative humidity.

system it is seen that in the absence of clay the gas permeability coefficient slightly increases after certain level of humidity due to saturation of the system while in the presence of clay such behavior is not observed due to barrier effect of clay. In addition, the polar nature of used clay can also play some role in water absorption.[43]

3.3. Phenomenological Models for Aspect Ratio Estimation

Platelet nanofillers aspect ratio (L/D) is a dominant factor in the tortuosity path against gas diffusion which can affect the permeability behavior of a filled system. Therefore, an in situ aspect ratio is defined as the criterion for aspect ratio within the matrix. Various models based on the tortuous path theory have been developed for estimating the aspect ratio or tortuosity factor. Some of the most common analytical models are presented in **Table 5**. Among these models, the Nielsen model[33] is the most simple one for predicting L/D of a filler. The Bharadwaj model has been developed and modified based on the Nielsen model.[35] In this model, the orientation of clay platelets, directly depending on sample preparation technique and the mixing conditions, is considered as a main characteristic that influences the clay aspect ratio. The other two models, known as Cussler models,[34] are used for disk type fillers; however, by a rough approximation they can be used for the platelet fillers too.[44]

The description of the Bharadwaj model as a typical example is as follows

$$\frac{D}{D_0}=\frac{1-\varphi}{1+\left(\frac{\alpha}{2}\right)\left(\frac{2}{3}\right)\left(S'+\frac{1}{2}\right)\varphi} \tag{3}$$

In the above equation, D_0 and D are the diffusivity of neat and filled samples, ϕ is the filler volume fraction, and α and S' are aspect ratio and orientation factor, respectively. The orientation factor (S') can assume three values of 0.5, 0, and

Table 5. Some of the analytical models for predicting clay aspect ratio.

Model	Formulae	Filler geometry	Ref.
Nielsen	$\frac{D}{D_0}=\frac{1-\varphi}{1+\frac{\alpha}{2}\varphi}$		[33]
Bharadwaj	$\frac{D}{D_0}=\frac{1-\varphi}{1+\left(\frac{\alpha}{2}\right)\left(\frac{2}{3}\right)\left(S'+\frac{1}{2}\right)\varphi}$		[35]
Cussler (regular orientation)	$\frac{D_0}{D}(1-\varphi)=1+\frac{(\alpha\varphi)^2}{4}$		[34]
Cussler (random orientation)	$\frac{D_0}{D}(1-\varphi)=\left(1+\frac{\alpha\varphi}{3}\right)^2$		[34]

Table 6. Aspect ratio of clay in the filled PLA/EVA blends based on the applied models.

Sample	Aspect ratio values					
	Nielsen	Bharadwaj			Cussler (rando)	Cussler (regular)
		$S' = 0$	$S' = 0.5$	$S' = 1$		
PLA/EVA/Cloisite 30B (75/25/5)	125	340	278	125	154	94
PLA/EVA/Cloisite 30B/PTW (75/25/5/5)	239	510	392	239	280	151
PLA/EVA/Cloisite 30B (25/75/5)	108	217	159	108	149	77

1 attributed to parallel, random and perpendicular arrangement of filler platelets against gas diffusion path, respectively. A favorable alignment of platelets exists in the matrix when $S' = 1$ which results in the highest barrier efficiency. The aspect ratio of clay was evaluated for the filled systems against nitrogen gas, as an inert and noninteracting gas, using all the four models and the results are summarized in **Table 6**.

As shown, the obtained aspect ratio values, as a criterion of clay dispersion state, vary in the investigated nanocomposite systems. All the applied analytical models predict a higher aspect ratio for the PLA-rich system as compared to the EVA-rich system implying a better dispersion state of clay in the PLA matrix. As discussed before, clay has better interaction with PLA than EVA, and it tends to localize mainly in the PLA phase, and therefore, it has better dispersion state and consequently a higher aspect ratio in the nanocomposite system in which PLA is the matrix. Incorporation of compatibilizer to the PLA-rich filled system leads to higher aspect ratio implying that the compatibilizer has improved the dispersion state of the filler. It is worth mentioning that the clay aspect ratio has a direct effect on the tortuosity path. The tortuosity increases with an increase in the filler aspect ratio which imposes a barrier effect against gas diffusion. Strong interfacial adhesion between filler and polymer has a significant effect on dispersion and aspect ratio of filler. These results are in agreement with the XRD, SEM, and TEM findings.

Figure 9 demonstrates the variation of relative diffusivity versus filler volume fraction for the noncompatibilized and compatibilized filled PLA-rich system calculated based on the obtained aspect ratio values using different models. As expected, the figures demonstrate that the relative permeability reduces with an increase in the filler volume fraction and the presence of compatibilizer leads to lower relative permeability values. Moreover, the Bhradwaj $S' = 0$ and the Cussler (regular) models predict the lowest and highest limits for the relative permeability values, respectively. The other models generate the curves which lie in between these two limits. It is to be noted that the discrepancy between the curves particularly at low filler volume fraction is higher than that at higher filler contents indicating that the filler orientation/dispersion state plays more important role when it is loaded at low quantities. Comparison of both set of the curves in Figure 9a,b reveals another important finding which the discrepancy between the models outputs particularly at low filler volume fraction is much lower when the compatibilizer added to the filled system. This indicates that the orientation of clay does not play significant role in permeability as a result of improved clay dispersion state due to compatibilizer which is in favor of random orientation of clay platelets.

4. Conclusion

The perm-selectivity of PLA- and EVA-rich blend nanocomposites in various compositions was determined for O_2, N_2, and CO_2 gases. The PLA-rich system exhibited significantly lower permeability than that of the EVA-rich system both at dry and humid conditions. The effect of nanoclay and compatibilizer incorporation on the gas permeability of the blends was investigated. Introducing nanoclay as a platelet filler in the PLA-rich system could significantly reduce the gas diffusion because of tortuosity effect, which prolongs the gas diffusion pathway. For a precise analysis of the tortuous path effect, N_2 permeability data fitted to analytical models to obtain filler aspect ratio in the nanocomposites. Incorporation of compatibilizer to the PLA-rich filled system led to higher aspect ratio implying that the compatibilizer has improved the dispersion state of the filler. Investigation of variation of relative diffusivity versus filler volume fraction for the noncompatibilized and compatibilized filled PLA-rich system calculated based on the obtained aspect ratio values using different models revealed that the filler orientation/dispersion state plays more important role when it is loaded at low quantities. It was also found that the orientation

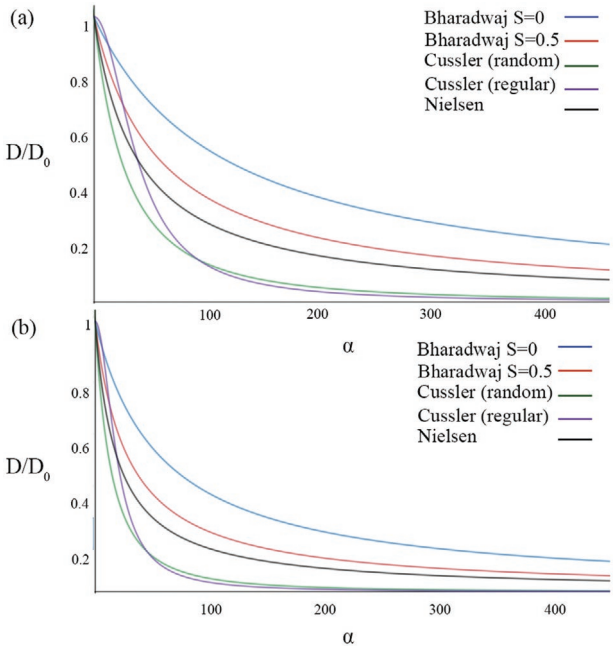

Figure 9. The variation of relative diffusivity versus filler volume fraction for a) 75/25/C5 and b) 75/25/C5/Co5.

of clay does not play significant role in permeability as a result of improved clay dispersion state due to compatibilizer which is in favor of random orientation of clay platelets. The microstructural analysis of the systems by scanning electron microscope, transmission electron microscopy and wide-angle X-ray scattering revealed that inclusion of compatibilizer to the filled blends, improved the blend morphology, dispersion state and intercalation level of clay platelets which were mainly localized at the interface of PLA/EVA immiscible phases and partly in the PLA phase. A correlation was established between the gas permeability and microstructure of the systems. Analysis of selectivity parameter (α), showed the lowest O_2 permeability and the highest CO_2/N_2 and O_2/N_2 selectivity which are favorable for a food packaging application. Investigation of gas permeability of the filled and nonfilled blends in the presence and absence of compatibilizer at humid conditions showed that the PLA-rich system was slightly more sensitive toward relative humidity as compared to the EVA-rich system attributed to more hydrophilic nature of PLA.

Acknowledgements

Open access funding enabled and organized by Projekt DEAL.

Conflict of Interest

The authors declare no conflict of interest.

Keywords

barrier films, bio-based film packaging, PLA/EVA blends, polymer/clay nanocomposites

Received: July 13, 2020
Revised: September 12, 2020
Published online: October 27, 2020

[1] C. Fan, R. Cui, W. Lu, H. Chen, M. Yuan, Y. Qin, *Polym. Test.* **2019**, *76*, 73.
[2] A. Salehi, S. H. Jafari, H. A. Khonakdar, H. Ebadi-Dehaghani, *J. Appl. Polym. Sci.* **2018**, *135*, 46665.
[3] M. R. Aghjeh, V. Asadi, P. Mehdijabbar, H. A. Khonakdar, S. H. Jafari, *Composites, Part B* **2016**, *86*, 273.
[4] J. R. Rocca-Smith, R. Pasquarelli, A. Lagorce-Tachon, J. Rousseau, S. Fontaine, V. Aguié-Béghin, F. Debeaufort, T. Karbowiak, *ACS Sustainable Chem. Eng.* **2019**, *7*, 3759.
[5] M. Razavi, M. Nazari, H. Ali, S. Hassan, U. Wagenknecht, G. Heinrich, *JMADE* **2015**, *88*, 1277.
[6] R. K. Singla, M. T. Zafar, S. N. Maiti, A. K. Ghosh, *Polym. Test.* **2017**, *63*, 398.
[7] H. Moustafa, A. M. Youssef, N. A. Darwish, A. I. Abou-Kandil, *Composites, Part B* **2019**, *172*, 16.
[8] E. M. B. Lima, A. M. Lima, A. P. S. Minguita, N. R. Rojas dos Santos, I. C. S. Pereira, T. T. M. Neves, L. F. da Costa Gonçalves, A. P. D. Moreira, A. Middea, R. Neumann, M. I. B. Tavares, R. N. Oliveira, *J. Appl. Polym. Sci.* **2019**, *136*, 47512.
[9] A. Khaki, H. Garmabi, A. Javadi, N. Yahyaee, *Eur. Polym. J.* **2019**, *118*, 53.
[10] N. Karimpour-Motlagh, H. A. Khonakdar, S. H. Jafari, M. Panahi-Sarmad, A. Javadi, S. Shojaei, V. Goodarzi, *Polym. Adv. Technol.* **2019**, *30*, 2695.
[11] P. Xu, P. Ma, M. Hoch, E. Arnoldi, X. Cai, W. Dong, M. Chen, *Polym. Degrad. Stab.* **2016**, *129*, 328.
[12] N. Karimpour-Motlagh, H. A. Khonakdar, S. M. A. Jafari, A. Mahjub, M. Panahi-Sarmad, S. F. Kasbi, S. Shojaei, V. Goodarzi, M. Arjmand, *Thermochim. Acta* **2020**, *691*, 178709.
[13] E. Číková, J. Kuliček, I. Janigová, M. Omastová, *Materials* **2018**, *11*, 1737.
[14] X. Wang, Z. He, J. Yang, N. Zhang, T. Huang, *Composites, Part A* **2016**, *91*, 105.
[15] P. Ma, D. G. Hristova-Bogaerds, J. G. P. Goossens, A. B. Spoelstra, Y. Zhang, P. J. Lemstra, *Eur. Polym. J.* **2012**, *48*, 146.
[16] N. Zhang, X. Lu, *Polym. Test.* **2016**, *56*, 354.
[17] R. Mirzaee, A. Aref-azar, *Polym. Test.* **2020**, *83*, 106346.
[18] C. Wolf, H. Angellier-coussy, N. Gontard, F. Doghieri, V. Guillard, *J. Membr. Sci.* **2018**, *556*, 393.
[19] B. Adak, B. S. Butola, M. Joshi, *Appl. Clay Sci.* **2018**, *161*, 343.
[20] B. Tan, N. L. Thomas, *Appl. Clay Sci.* **2017**, *141*, 46.
[21] N. Tenn, N. Follain, J. Soulestin, R. Crétois, S. Bourbigot, S. Marais, *J. Phys. Chem. C* **2013**, *117*, 12117.
[22] H. Adelnia, H. C. Bidsorkhi, A. F. Ismail, T. Matsuura, *Sep. Purif. Technol.* **2015**, *146*, 351.
[23] V. Goodarzi, S. Hassan Jafari, H. Ali Khonakdar, B. Ghalei, M. Mortazavi, *J. Membr. Sci.* **2013**, *445*, 76.
[24] S. Singha, R. Koyilapu, K. Dana, T. Jana, *Polymer* **2019**, *167*, 13.
[25] S. Xia, X. Liu, J. Wang, Z. Kan, H. Chen, W. Fu, Z. Li, *Composites, Part B* **2019**, *168*, 398.
[26] H. Koolivand, A. Sharif, M. R. Kashani, M. Karimi, M. K. Salooki, M. A. Semsarzadeh, *J. Polym. Res.* **2014**, *21*, 599.
[27] M. Raef, M. Razzaghi-Kashani, *Polymer* **2019**, *182*, 121816.
[28] E. Chehrazi, M. Raef, M. Noroozi, M. Panahi-Sarmad, *J. Membr. Sci.* **2019**, *570-571*, 168.
[29] E. Chehrazi, A. Sharif, M. Omidkhah, M. Karimi, *ACS Appl. Mater. Interfaces* **2018**, *10*, 16925.
[30] T. Messin, S. Marais, N. Follain, C. Chappey, A. Guinault, G. Miquelard-Garnier, N. Delpouve, V. Gaucher, C. Sollogoub, *Eur. Polym. J.* **2019**, *111*, 152.
[31] M. Bhattacharya, S. Biswas, A. K. Bhowmick, *Polymer* **2011**, *52*, 1562.
[32] Y. Cui, S. I. Kundalwal, S. Kumar, *Carbon* **2016**, *98*, 313.
[33] L. E. Nielsen, *J. Macromol. Sci., Part A: Pure Appl. Chem.* **1967**, *1*, 929.
[34] E. L. Cussler, S. E. Hughes, W. J. Ward, R. Aris, B. membranes, *J. Membr. Sci.* **1988**, *38*, 161.
[35] R. K. Bharadwaj, *Macromolecules* **2001**, *34*, 9189.
[36] G. Choudalakis, A. D. Gotsis, *Eur. Polym. J.* **2009**, *45*, 967.
[37] K. Wang, Y. Chen, Y. Zhang, *Polymer* **2008**, *49*, 3301.
[38] G. Ait Cherif, A. Kerkour, T. Baouz, I. Pillin, Y. Grohens, *Packag. Technol. Sci.* **2018**, *31*, 621.
[39] M. Entezam, D. Nozari, M. Mirjalili, H. A. Khonakdar, *Polym.-Plast. Technol. Eng.* **2015**, *54*, 1571.
[40] S. Adrar, A. Habi, A. Ajji, Y. Grohens, *Appl. Clay Sci.* **2018**, *157*, 65.
[41] J. Baltrusaitis, J. Schuttlefield, E. Zeitler, V. H. Grassian, *Chem. Eng. J.* **2011**, *170*, 471.
[42] F. Johansson, *Foods Packag. Mater. Chem. Interact.* **1994**, *59*, 1328.
[43] H. Alamri, I. M. Low, *Composites, Part A* **2013**, *44*, 23.
[44] G. H. Fredrickson, J. Bicerano, *J. Chem. Phys.* **1999**, *110*, 2181.